

Crystal-chemical implications of the Mg^{2+} – Fe^{2+} distribution in orthopyroxenes

M. CHIARA DOMENEGHETTI,

*C.N.R. Centro di Studio per la Cristallografia Strutturale
c/o Dipartimento di Scienze della Terra
Universita' di Pavia, Via Bassi 4, 27100 Pavia, Italy*

G. MARIO MOLIN

*C.N.R. Centro di Studio per i problemi dell'Orogeno delle Alpi Orientali
c/o Istituto di Mineralogia e Petrologia, Universita' di Padova
Corso Garibaldi 37, 35100 Padova, Italy*

AND VITTORIO TAZZOLI

*C.N.R. Centro di Studio per la Cristallografia Strutturale
c/o Dipartimento di Scienze della Terra
Universita' di Pavia, Via Bassi 4, 27100 Pavia, Italy*

Abstract

Structure refinement data of natural and heated orthopyroxenes with different Fe/(Fe + Mg) ratios were used for a systematic analysis of structural variations as a function of chemical composition and ordering degree. The mean T–O bond distances do not vary significantly with increasing iron content and therefore any change of $\langle TB-O \rangle$ distances may provide a measure of Si/Al^{IV} substitution, which occurs only at the TB site. The mean M1–O distance increases linearly with iron content as a consequence of a homogeneous expansion of M1 site. The mean M2–O distance also increases with iron content, but the linear plot is the sum of very different trends of the individual bond lengths; among these, the M2–O3 distances exhibit a peculiar behavior consistent with a 4 + 2 coordination of the M2 polyhedron. The R³⁺ cations, which enter the structure with the Si/Al^{IV} substitution, appear to order totally in the M1 site.

Introduction

A crystal-chemical study of Mg^{2+} – Fe^{2+} order–disorder in orthopyroxenes was undertaken by using X-ray diffraction techniques. The data obtained in natural and heated (disordered) samples allow a systematic analysis of structural variation as a function of order–disorder and chemical composition.

All the crystal-chemical data published on pyroxenes until 1980 was exhaustively reviewed by Cameron and Papike (1981). The structure of *Pbca* orthopyroxenes consists of alternating tetrahedral and octahedral layers. The tetrahedral layers show two non-equivalent tetrahedra TA and TB (TA smaller and more distorted than TB). These are linked in A and B chains respectively, parallel to *c*, to form A and B layers parallel to the (100) plane. O-rotation occurs in both chains and a violation of the parity rule occurs in the A layer (Thompson, 1971). The octahedral layers consist of zig-zag chains of regular M1 octahedra, parallel to *c* and joined by larger and distorted M2 polyhedra. Si/Al^{IV} substitution occurs only in TB. Mg^{2+} and

Fe^{2+} prefer M1 and M2 respectively; the Mg^{2+} – Fe^{2+} partitioning between M1 and M2 depends on the Mg/Fe ratio in the crystal and on temperature, which controls the exchange reaction $Mg^{2+}(M1) + Fe^{2+}(M2) \rightleftharpoons Fe^{2+}(M1) + Mg^{2+}(M2)$. The larger cations such as Ca^{2+} and Mn^{2+} prefer M2; Cr^{3+} , Al^{VI} and Fe^{3+} prefer M1, but no convincing evidence has been reported to date for the R³⁺ cations distribution between M1 and M2.

We have carried out crystal structure refinements at room temperature of natural and heated crystals taken from three rock samples labelled 274, 10 and 10/68 (Saxena and Ghose, 1971).

The samples were chosen to cover a wide range of Fe/(Fe + Mg) ratios and to avoid as much as possible the presence of minor elements. Among them, aluminum plays a peculiar role because even in small amounts it causes significant changes in some structure parameters of orthopyroxenes. Therefore, the presence of a small amount of Al^{IV} (see Table 1) in sample 10 required a comparison with some unpublished data on aluminous orthopyroxenes

Table 1. Electron microprobe analyses of orthopyroxenes

Wt%	274	10	10/68
SiO ₂	55.80	50.94	49.00
Al ₂ O ₃	0.00	0.66	0.00
FeO	11.38	27.52	42.36
MgO	29.15	17.98	7.74
MnO	2.92	1.13	1.39
TiO ₂	0.00	0.00	0.00
Cr ₂ O ₃	0.00	0.00	0.00
CaO	0.33	0.68	0.84
Na ₂ O	0.00	0.00	0.00
Sum	99.58	98.91	101.33
a. f. u.			
Si ^{IV}	2.000	1.974	1.999
Al ^{IV}	0.000	0.026	0.000
	2.000	2.000	1.999
Al ^{VI}	0.000	0.004	0.000
Fe ²⁺	0.341	0.870	1.446
Fe ³⁺	0.000	0.022	0.000
Mg	1.557	1.039	0.470
Mn	0.089	0.037	0.048
Ti	0.000	0.000	0.000
Cr	0.000	0.000	0.000
Ca	0.013	0.028	0.037
Na	0.000	0.000	0.000
	2.000	2.000	2.001
Fe/Fe+Mg	0.180	0.462	0.755
Fe ²⁺ /Fe ³⁺ partitioned according to Papike et al., 1974.			

(from ultramafic nodules of Victoria, Australia; A. Dal Negro pers. comm., 1984; see Table 2). Structural parameters of synthetic enstatite (Ganguly and Ghose, 1979) and of synthetic ferrosilite (Sueno et al., 1976) were also plotted in the diagrams of this paper.

Experimental

Samples

The following samples were used: (1) Opx 274: Fe/(Fe + Mg) = 0.180 Iron Formation, Gagnon Region, Canada (Butler, 1969); (2) Opx 10: Fe/(Fe + Mg) = 0.462 Arendalite, Norway (collected by Saxena); (3) Opx 10/68: Fe/(Fe + Mg) = 0.755 Charnokite, Varberg, Sweden (Saxena, 1968).

Procedures

The following procedure was applied to every crystal:

(1) X-ray data collection and structure refinement of the natural crystal;

(2) a series of heating experiments conducted on the same crystal at 700°C until it reached a close approach to the Mg^{2+} - Fe^{2+} exchange equilibrium; X-ray data collection and structure refinement after every heating;

(3) microprobe analysis of the same crystal, after the last X-ray

data collection. Temperature and duration of heatings are reported in Tables 3, 4 and 5.

X-ray single crystal diffractometry

X-ray diffraction data were collected with a Philips PW 1100 four circle diffractometer, using graphite monochromated MoK α radiation. The equivalent pairs hkl and $\bar{h}kl$ were measured up to $\theta \leq 30^\circ$ using the ω -scan mode.

The intensities were corrected for absorption following the semi-empirical method of North et al. (1968) and the values of equivalent pairs were averaged.

The resulting discrepancy factors: $R_{sym} =$

$$\frac{\sum_{hkl}(I_{hkl} - \bar{I})/\sum_{hkl}\bar{I}}{\text{where } \bar{I} = (I_{hkl} + I_{\bar{h}kl})/2}$$

range between 1.5 and 2.8%.

The unit-cell parameters were determined using a locally improved version (Cannillo et al., 1983) of the Philips LAT routine.

Structure refinement

The refinements were carried out in space group $Pbca$ without chemical constraints using a locally rewritten version of the program ORFLS (Busing et al., 1962). The program allows assignment to every site involved in isomorphous replacements of two scattering curves $f1$ and $f2$ and refinement of the occupancy factors $x(f)$ with the constraint that $x(f1) + x(f2) = 1$. The adopted ionization scheme (Rossi et al., 1983) was 2.0 positive charges for Si, 1.5 negative charges for oxygens and complete ionization for Mg and Fe. The atomic scattering curves were taken from the *International Tables for X-Ray Crystallography* (1974) and, for O^{2-} , from Tokonami (1965).

The reflections with $I \geq 3\sigma(I)$ were considered as observed, and were utilized for the refinements with equal weight. The extinction correction of Coppens and Hamilton (1970) was applied. All the atoms were treated anisotropically, starting with the atomic and thermal parameters of Ganguly and Ghose (1979). All the parameters were varied simultaneously during the refinements and no correlation greater than 0.7 was observed. All the final difference Fourier maps were featureless. Final atomic parameters and observed and calculated structure factors are available in Tables 6a to 6i.¹

A preliminary systematic examination of the correlations between structural parameters was carried out using program CORORTO (E. Cannillo, pers. comm., 1983).

Heating experiments

The crystals were sealed in small quartz tubes under a nitrogen pressure of 1 atm, in the presence of iron fillings to catch residual oxygen, and were then heated in a temperature-controlled furnace ($\pm 3^\circ C$, Pt/Pt-Rh thermocouple). Quenching of the crystals was done by dropping the tubes into cold water. The total quenching time from 700°C to 25°C was estimated to be ca. one second.

Table 2. Al content in Al-rich samples of orthopyroxenes

	LE 8	LE 11	LE 4
Al ₂ O ₃ (wt %)	0.91	2.17	4.02
Al ^{IV} (a. f. u.)	0.030	0.052	0.110
Al ^{VI} (a. f. u.)	0.007	0.036	0.053

Table 3. Crystal and refinement data (space group: *Pbca*)

Sample	a(Å) (+0.004)	b(Å) (+0.002)	c(Å) (+0.001)	V(Å ³)	N. of I(obs)	N. of I(all)	R _{sym} * x100	R _{obs} ** x100	R _{all} ** x100
274	18.278	8.863	5.201	842.6	779	1116	2.30	1.95	4.41
274 4h 700°C	18.281	8.865	5.201	842.9	767	1101	2.80	2.54	4.96
274 100h 700°C	18.285	8.867	5.202	843.4	730	967	2.60	2.01	3.48
10	18.312	8.909	5.220	851.6	936	1214	2.10	1.89	2.98
10 15m 700°C	18.326	8.915	5.221	853.0	870	1209	1.90	1.60	4.01
10 45m 700°C	18.325	8.914	5.221	852.8	876	1211	2.30	1.75	3.39
10/68	18.384	9.002	5.236	866.5	905	1245	1.50	1.61	2.91
10/68 10m 700°C	18.398	9.003	5.238	867.6	905	1246	2.10	1.94	3.42
10/68 20m 700°C	18.396	9.006	5.237	867.6	892	1248	1.50	1.43	2.93

*R_{sym} refers to the agreement between the intensity measurement of the equivalent pairs hkl and $\bar{h}\bar{k}\bar{l}$:

$$R_{\text{sym}} = \frac{\sum_{hkl} (I_{hkl} - \bar{I})}{\sum_{hkl} \bar{I}} \quad \text{where } \bar{I} = (I_{hkl} + I_{\bar{h}\bar{k}\bar{l}}) / 2$$

**R_{obs} and R_{all} are the final conventional discrepancy indices expressed as $\frac{\sum ||F_o| - |F_c||}{\sum |F_o|}$

Microprobe analyses

An energy dispersive spectrometer EDS EG&G connected to a SEM AUTOSCAN electron microscope operating at 15 kv was employed to analyze the single-crystals. A MAGIC program (Colby, 1967) in the ORTEC MAGIC IV M. version was used to convert X-ray counts into oxide weight percent. The analyses reported in Table 1 refer to the same three crystals used for X-ray data collection and heating experiments. They are averaged over 4 to 6 spots for every crystal; all the crystals were rather homogeneous.

Results and discussion

Chemical analyses are reported in Table 1; crystal-chemical data in Tables 3, 4 and 5.

Tetrahedra

The variations in the T-O bond lengths, the distortion of the tetrahedra and the kinking of the chains (Table 4) are correlated with the iron content deduced by site occupancy refinement (Table 5).

The tetrahedral bond lengths are plotted against $X_{\text{Fe}^{2+}(\text{M1})} + X_{\text{Fe}^{2+}(\text{M2})}$, i.e., against total Fe²⁺ content, in Figure 1. In Al-free orthopyroxenes both TA and TB tetrahedra show a slight shortening of the (T-O) bridging distances and a concomitant slight lengthening of the <T-O> non-bridging distances with increasing total iron. The net result is that the <TA-O> and <TB-O> distances are not significantly modified by any variation of total iron. It is also evident from the plots that Si/Al^{IV} substitution occurs only in the TB site, where both <T-O> bridging and <T-O> non-bridging distances increase significantly with increasing Al content (see LE 4, LE 8, LE 11 and 10 samples). In the TA site, only the <T-O> non-bridging distances increase slightly: but this is due to the shortening of

the M1-O1 and M1-O2 bond lengths, due to the presence of R³⁺ cations in M1 (see below). As the <TB-O> distance is not influenced by the octahedral population, it may be a reliable parameter for measuring the amount of Si/Al^{IV} substitution in orthopyroxenes. No appreciable changes of T-O bond lengths are noted with increasing Mg-Fe²⁺ disorder in the crystals.

The tetrahedral quadratic elongation (TQE, Robinson et al., 1971) shows a significant decrease in TA with increasing iron content (see Table 4). This is mainly due to an increase in the angle O2A-Si-O3A as a consequence of the lengthening of the edge O2A-O3A, shared between the TA and M2 sites. Nevertheless the edge O2A-O3A always remains remarkably short, ranging from 2.489Å in enstatite to 2.514Å in ferrosilite. The TB tetrahedron, which does not share any edge with other polyhedra, shows very small variations of TQE with increasing iron content; also the presence of Al^{IV} does not affect this parameter significantly.

The kinking of the chains varies significantly with the total iron content as shown in Figure 2. The O3-O3-O3 angles increase in both chains with total iron as the unit-cell parameter *c* increases. The straightening of the chains is caused by the expansion of the octahedral layer with respect to the tetrahedral layer. It is worth noting that similar behavior, but due to thermal expansion, was described by Smyth (1973) in an iron-rich orthopyroxene. The O3A-O3A-O3A angle is more affected by the total iron content than O3B-O3B-O3B because of the smaller dimension of the TA tetrahedra. At a constant iron content the presence of Al^{IV} does not influence the O3A-O3A-O3A angle but it causes a decrease of the O3B-O3B-O3B angle, because of the increase in the size of TB.

The disorder induced by heating causes a small contrac-

Table 4. Interatomic distances (e.s.d. $\leq 0.002\text{\AA}$), relevant angles (e.s.d. in parentheses) and other geometrical parameters* of tetrahedra and octahedra

	274	274	274	10	10	10	10/68	10/68	10/68
		4h 700°C	100h 700°C		15m 700°C	45m 700°C		10m 700°C	20m 700°C
SiA-01A	1.608	1.609	1.611	1.611	1.612	1.610	1.610	1.614	1.612
-02A	1.589	1.595	1.596	1.598	1.595	1.596	1.600	1.600	1.598
-03A	1.644	1.641	1.642	1.637	1.638	1.635	1.634	1.638	1.638
-03A	1.659	1.663	1.662	1.656	1.657	1.659	1.655	1.653	1.653
< SiA-O >	1.625	1.627	1.628	1.625	1.625	1.625	1.625	1.626	1.625
Mean br.	1.651	1.652	1.652	1.646	1.647	1.647	1.644	1.645	1.645
Mean n.br.	1.598	1.602	1.603	1.604	1.603	1.603	1.605	1.607	1.605
$V(\text{\AA}^3)$	2.174	2.182	2.186	2.178	2.178	2.177	2.177	2.182	2.179
TQE	1.0088	1.0090	1.0089	1.0081	1.0082	1.0081	1.0073	1.0071	1.0077
TAV($^\circ$)	35.89	36.86	36.40	33.43	33.56	33.31	30.21	31.60	31.60
TILT($^\circ$)	3.84	3.86	3.83	4.04	4.05	4.13	4.26	4.36	4.18
O2A-SiA-03A	100.39(8)	100.08(11)	100.10(9)	100.80(7)	100.64(6)	100.75(7)	100.14(7)	100.83(9)	100.87(6)
O3A-03A-03A	162.23(14)	162.00(18)	161.95(14)	166.16(12)	165.51(11)	165.67(11)	168.49(12)	167.79(16)	167.70(11)
SiB-01B	1.620	1.621	1.619	1.624	1.623	1.625	1.621	1.621	1.619
-02B	1.587	1.589	1.587	1.601	1.600	1.600	1.602	1.598	1.600
-03B	1.668	1.673	1.671	1.672	1.673	1.673	1.668	1.670	1.668
-03B	1.674	1.671	1.675	1.666	1.667	1.668	1.664	1.664	1.667
< SiB-O >	1.637	1.638	1.638	1.641	1.641	1.642	1.639	1.638	1.638
Mean br.	1.671	1.672	1.673	1.669	1.670	1.670	1.666	1.667	1.667
Mean n.br.	1.603	1.605	1.603	1.612	1.611	1.612	1.611	1.609	1.609
$V(\text{\AA}^3)$	2.237	2.242	2.241	2.252	2.251	2.256	2.244	2.241	2.243
TQE	1.0051	1.0050	1.0051	1.0047	1.0049	1.0048	1.0046	1.0048	1.0046
TAV($^\circ$)	19.22	18.82	19.15	18.32	18.98	18.40	17.74	18.22	17.68
TILT($^\circ$)	6.57	6.55	6.61	5.97	6.29	6.32	6.32	6.49	6.36
O2B-SiB-03B	105.16(8)	105.01(11)	105.15(9)	105.04(7)	104.84(7)	104.96(7)	105.02(7)	104.93(9)	104.97(7)
O3B-03B-03B	141.80(12)	141.49(16)	141.57(12)	143.47(11)	142.91(10)	142.62(10)	144.64(10)	144.21(13)	144.23(9)
M1-01A	2.034	2.036	2.037	2.033	2.040	2.042	2.062	2.066	2.066
-01A	2.149	2.151	2.154	2.148	2.156	2.157	2.172	2.175	2.174
-01B	2.175	2.175	2.176	2.166	2.169	2.170	2.185	2.188	2.188
-01B	2.061	2.064	2.066	2.061	2.072	2.072	2.092	2.098	2.099
-02A	2.022	2.020	2.020	2.042	2.045	2.043	2.068	2.068	2.070
-02B	2.060	2.060	2.058	2.066	2.068	2.069	2.094	2.098	2.100
< M1-O >	2.084	2.084	2.085	2.086	2.092	2.092	2.112	2.115	2.116
$V(\text{\AA}^3)$	11.931	11.941	11.950	11.973	12.070	12.075	12.426	12.478	12.491
OQE	1.0081	1.0083	1.0083	1.0078	1.0080	1.0080	1.0081	1.0083	1.0081
OAV($^\circ$)	24.37	25.10	25.09	23.98	24.77	24.90	25.39	26.09	25.62
M2-01A	2.134	2.131	2.129	2.170	2.162	2.162	2.167	2.162	2.165
-01B	2.097	2.092	2.092	2.124	2.117	2.112	2.129	2.125	2.126
-02A	2.057	2.051	2.050	2.056	2.055	2.054	2.044	2.042	2.043
-02B	1.996	1.995	2.000	2.005	2.001	2.000	2.002	2.001	2.000
-03A	2.326	2.322	2.322	2.379	2.375	2.377	2.430	2.424	2.424
-03B	2.487	2.485	2.485	2.510	2.505	2.501	2.573	2.572	2.569
< M2-O > of 6	2.183	2.179	2.180	2.207	2.202	2.201	2.224	2.221	2.221
< M2-O > of 4	2.071	2.067	2.068	2.089	2.084	2.082	2.086	2.083	2.084
$V(\text{\AA}^3)$	12.883	12.836	12.846	13.195	13.138	13.121	13.448	13.403	13.406
OQE	1.0567	1.0561	1.0557	1.0641	1.0625	1.0620	1.0692	1.0684	1.0683
M2-M1	2.981	2.980	2.978	2.996	2.996	2.995	3.067	3.067	3.066
M2-TA	2.831	2.831	2.830	2.856	2.855	2.854	2.874	2.875	2.874
M2-TB	3.134	3.139	3.141	3.126	3.134	3.135	3.132	3.135	3.126
O2A-03A	2.495	2.498	2.498	2.507	2.503	2.508	2.514	2.507	2.507
O2B-03B	2.586	2.589	2.588	2.598	2.594	2.597	2.595	2.592	2.592
O3A-03A	2.632	2.633	2.634	2.629	2.631	2.631	2.631	2.634	2.634
O3B-03B	2.752	2.755	2.754	2.749	2.753	2.756	2.748	2.752	2.751

*TQE (tetrahedral quadratic elongation) = $\frac{4}{3} \sum_{i=1}^4 (l_i/l_o)^2/4$ where l_o is the center-to-vertex distance for a regular tetrahedron whose volume is equal to that of real tetrahedron with bond lengths l_i . TAV (tetrahedral angle variance) = $\frac{6}{5} \sum_{i=1}^6 (A_i - 109.47)^2/5$ where A_i 's are the tetrahedral angles O-T-O. TILT is the out-of-plane tilting of the basal face of the tetrahedra and the plane (100). OQE (octahedral quadratic elongation) = $\frac{6}{5} \sum_{i=1}^6 (l_i/l_o)^2/6$ where l_o is the center-to-vertex distance for a regular octahedron whose volume is equal to that of a real octahedron with bond lengths l_i . OAV (octahedral angle variance) = $\frac{12}{5} \sum_{i=1}^12 (A_i - 90)^2/11$ where A_i 's are the angles O-M-O (Robinson et al., 1971).

Table 5. Site populations in M1 and M2 sites

Sample	$X_{Mg}^{(M1)}$	$X_{Fe^{2+}}^{(M1)}$	$X_{Fe^{2+}}^{(M2)}$	$X_{Mg}^{(M2)}$	$X_{Fe^{2+}}^{(M1)} + X_{Fe^{2+}}^{(M2)}$
274	0.982 (9)	0.018 (9)	0.420 (10)	0.580 (10)	0.438
274 4h 700°C	0.948 (11)	0.052 (11)	0.380 (12)	0.620 (12)	0.432
274 100h 700°C	0.932 (9)	0.068 (9)	0.371 (10)	0.629 (10)	0.439
10	0.882 (8)	0.118 (8)	0.868 (10)	0.132 (10)	0.986
10 15m 700°C	0.757 (7)	0.243 (7)	0.747 (8)	0.253 (8)	0.990
10 45m 700°C	0.737 (8)	0.263 (8)	0.723 (9)	0.277 (9)	0.986
10/68	0.438 (9)	0.562 (9)	0.975 (10)	0.025 (10)	1.537
10/68 10m 700°C	0.373 (11)	0.627 (11)	0.908 (12)	0.092 (12)	1.535
10/68 20m 700°C	0.377 (8)	0.623 (8)	0.909 (9)	0.091 (9)	1.532

The numbers in parentheses (= e.s.d. x 3) give a realistic evaluation of the accuracy of the method.

tion of O3–O3–O3 angles (see Table 4); however this variation is not accompanied by a shortening of the c unit-cell parameter and it is correlated with a small lengthening of the O3–O3 edges.

M1 polyhedron

The M1 site is a nearly regular octahedron and its distortion, defined by the parameter OQE (Robinson et al., 1971), does not vary significantly from the mean value of 1.008 with increasing $X_{Fe^{2+}}^{(M1)}$ (Table 4).

All the individual M1–O bond lengths increase with iron content. Thus in the R^{3+} poor samples the $\langle M1-O \rangle$ bond length (Fig. 3) shows a fairly linear correlation with $X_{Fe^{2+}}^{(M1)}$ in agreement with the results of Morimoto and Koto (1969). It can be noted that sample 10, characterized by a $Fe/(Fe + Mg)$ of 0.46, lies close to sample 274 with a $Fe/(Fe + Mg)$ of 0.18 due to the ordering of Fe^{2+} in the M2 site (see the pattern of the Mg^{2+} - Fe^{2+} distribution between M1 and M2 in orthopyroxenes, Saxena and Ghose, 1971).

In heating experiments the displacement of Fe^{2+} from M2 to M1 is accompanied by an increase in the $\langle M1-O \rangle$ bond length. This increase shows the same slope as for the natural series: this suggests that temperature and Fe/Mg composition have similar effects on the size of the M1 polyhedron, which depends only on its own site population.

In the Al^{IV} -rich samples the presence of R^{3+} cations, which balances the Si/Al^{IV} substitution, clearly affects the $\langle M1-O \rangle$ distance, which shows a shortening proportional to the R^{3+} content.

M2 polyhedron

The M2 site is a distorted polyhedron and the plots of the individual M2–O bond lengths vs. $X_{Fe^{2+}}^{(M2)}$ show dif-

ferent shapes. The M2–O2A and M2–O2B distances are the shortest and least affected whereas M2–O3A and M2–O3B are the longest and the most variable.

M2–O1 bond lengths. The M2–O1B bond distance in

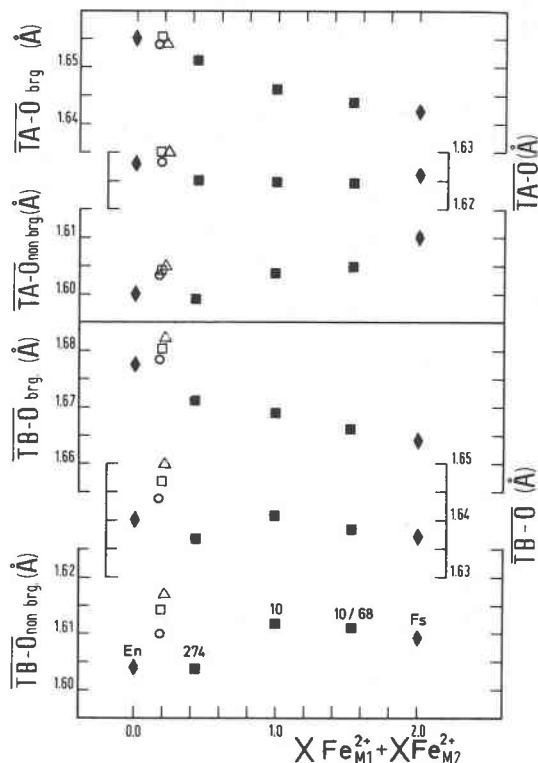


Fig. 1. Variation of mean tetrahedral bond lengths with total Fe^{2+} content. Solid symbols: squares, present paper unheated samples 274, 10, 10/68; (see Tables 4 and 5) diamonds, synthetic enstatite (Ganguly and Ghose, 1979) and ferrosilite (Sueno et al., 1976). Open symbols represent aluminous orthopyroxenes of ultramafic nodules from Victoria, Australia (A. Dal Negro, pers. comm., 1984); circle LE 8, square LE 11, triangle LE 4, with Al^{IV} content of 0.030, 0.052 and 0.110 respectively (Table 2).

¹ To obtain a copy of Tables 6a to 6i, order Document AM-85-277 from the Business Office, Mineralogical Society of America, 2000 Florida Avenue, N.W., Washington, D.C. 20009. Please remit \$5.00 in advance for the microfiche.

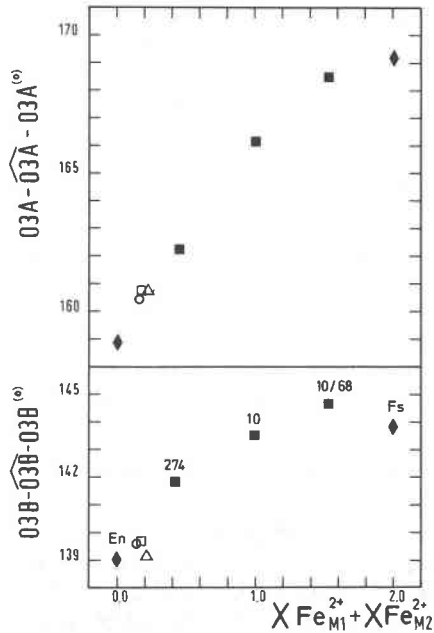


Fig. 2. Variation of O3-O3-O3 angles in A and B chains with total Fe^{2+} content. Same symbols as for Fig. 1.

Al-rich and Al-free orthopyroxenes increases regularly with iron content (Fig. 4) whereas the data in the corresponding M2-O1A plot are more scattered. Also in these diagrams the position of sample 10, now lying close to 10/68, reflects the distribution of Fe^{2+} between M2 and M1. Samples with the highest Al^{IV} , and consequently the highest R^{3+} content, show longer M2-O1A bond distance compared with that of samples without Al^{IV} . The different behavior

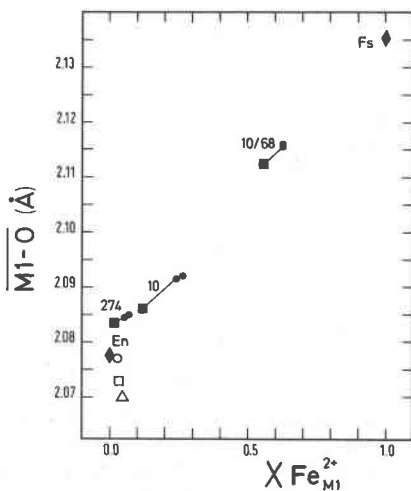


Fig. 3. Variation of mean M1-O bond length with Fe^{2+} content of M1 site. Same symbols as for Fig. 1; solid circles connected to the solid square represent the same crystal after heating experiments (see Tables 4 and 5).

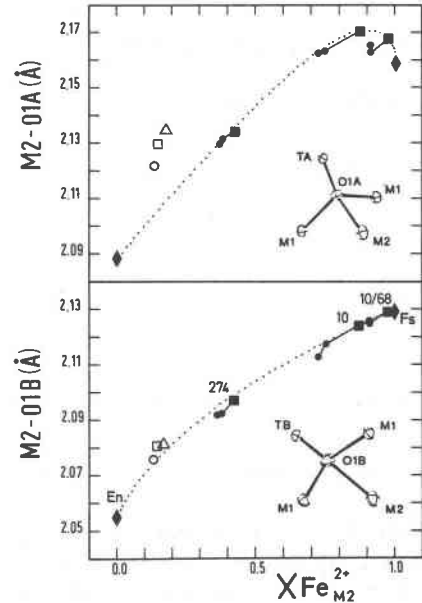


Fig. 4. Variation of M2-O1A and M2-O1B bond lengths with Fe^{2+} content of M2 site. Same symbols as for Fig. 3. The insets sketch the environment of the oxygens O1A and O1B.

between the M2-O1A and M2-O1B distances in Al^{IV} -rich samples can be explained by the different environment of the oxygens O1A and O1B (see insets to Fig. 4). The contraction of the M1-O1B distance, due to R^{3+} cations in M1, is compensated by the lengthening of the TB-O1B bond (due to the entry of Al^{IV} in TB) whereas the shortening of the M1-O1A distance is essentially balanced by a lengthening of the M2-O1A bond, TA-O distances being constant.

The negative slope of the curves of Figure 4, in the range of the more Fe-rich samples, is strictly related to the steep slope in the same region of the plots of M2-O3A and M2-O3B vs. $X_{Fe^{2+}}(M2)$ (see below).

M2-O2 bond lengths. The two shortest distances of the M2 site, M2-O2A and M2-O2B, involve the underbonded oxygens O2 and therefore they show little variation with $X_{Fe^{2+}}(M2)$. Nevertheless the distribution of the points in the plots of Figure 5 shows some analogies with that of Figure 4. The explanation is similar: the lengthening of the M2-O2A distances in the Al^{IV} -rich samples is caused by the presence of R^{3+} cations in M1, whereas the shape of both curves is related to that of the variation in M2-O3A and M2-O3B vs. $X_{Fe^{2+}}(M2)$.

M2-O3 bond lengths. M2-O3A and M2-O3B are the longest distances of the M2 polyhedron, with M2-O3A ranging from 2.29Å in enstatite to 2.46Å in ferrosilite and M2-O3B from 2.45Å to 2.60Å, respectively. These values seem to be very high for an octahedral Fe^{2+} and Mg^{2+} coordination. Furthermore the curves of the plots M2-O3A vs. $X_{Fe^{2+}}(M2)$ and M2-O3B vs. $X_{Fe^{2+}}(M2)$ in Figure 6 show a peculiar shape: the distances increase with

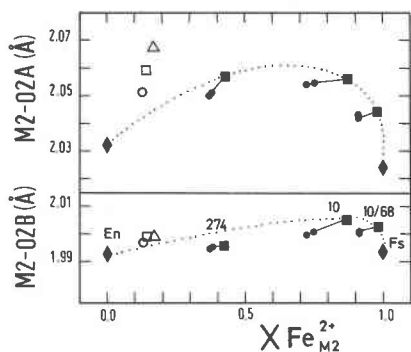


Fig. 5. Variation of M2-O2A and M2-O2B bond lengths with Fe^{2+} content of M2 site. Same symbols as for Fig. 3.

increasing $X_{Fe^{2+}}(M2)$ but the slope of the curves becomes surprisingly steep near the ferrosilite pole. The reason is that the lengthening of the distances M2-O3 is mainly due to an increase of $Fe^{2+}(M2)$ in the Fe-poor orthopyroxenes and to an increase of $Fe^{2+}(M1)$ in the more Fe-rich samples, while the M2 site is already iron-saturated. In other words M2-O3A and M2-O3B are initially controlled by $X_{Fe^{2+}}(M2)$ and then by $X_{Fe^{2+}}(M1)$, or by the site population and consequently by the dimensions of the entire octahedral layer. This is confirmed by the high linear corre-

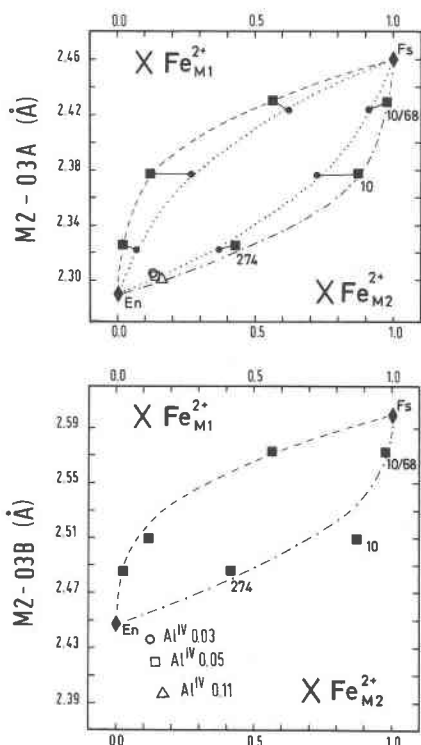


Fig. 6. Variation of M2-O3A and M2-O3B bond lengths with Fe^{2+} content of M2 site (lower curve) and Fe^{2+} content of M1 site (upper curve); same symbols as for Fig. 3. Dotted lines represent the maximum disorder reached at 700°C.

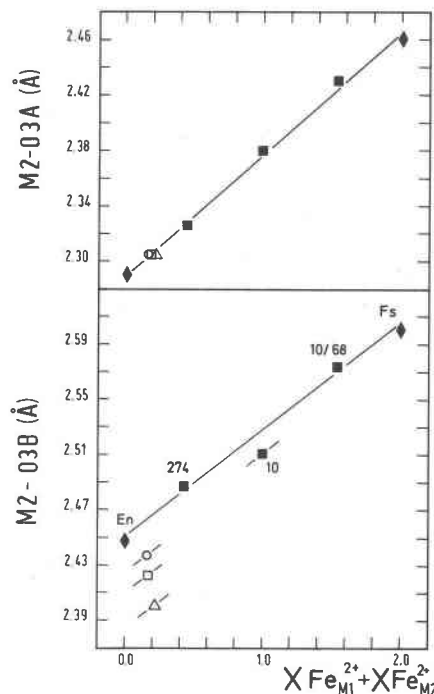


Fig. 7. Variation of M2-O3A and M2-O3B bond lengths with total Fe^{2+} content. Same symbols as for Fig. 1. The correlation coefficients are respectively 0.999 and 0.998 (the second one is obviously calculated among Al-free samples).

lations (Fig. 7) between M2-O3A and M2-O3B and $X_{Fe^{2+}}(M2) + X_{Fe^{2+}}(M1)$ (correlation coefficients $R = 0.999$ and $R = 0.998$ respectively).

The expansion of the octahedral layer causes, as previously reported, a lengthening of the tetrahedral chains by increasing the O3-O3-O3 angles (Fig. 2) and the unit-cell parameter c . Consequently the M2-O3A and M2-O3B bond lengths are strictly related to the position reached by the oxygens O3A and O3B because of the straightening of the chains. This position appears to be only slightly controlled by the cations occupying the M2 site. Accordingly, the steep increase of Fe^{2+} in M1 in the more Fe-rich samples, which moves the O3 oxygens away from M2, causes a slight charge imbalance at this site, which is compensated by a shortening of the M2-O1 and M2-O2 distances (Figs. 4 and 5). On the basis of these arguments M2 in *Pbca* orthopyroxenes has to be considered a site with a 4 + 2 coordination, in agreement with the results obtained by Smyth (1973) from high temperature structure refinements.

The low bond strength between M2 and O3 makes it more difficult to explain the short edge O2A-O3A on the basis of Pauling's (1960) rules concerning the cation-cation repulsion in edge-sharing polyhedra.

As far as the Al^{IV} -rich members are concerned, it appears from plots of Figure 6 that the M2-O3B bond distance (and not M2-O3A) decreases with increasing Al^{IV} content.

$\langle M2-O \rangle$ bond length. The plot of the mean M2-O distance vs. $X_{Fe^{2+}(M2)}$ shows a fairly linear positive trend (Fig. 8). The linearity of this plot is not caused, as for M1, by a linear variation of each individual bond length but by the sum of their previously mentioned complementary trends due to local charge balance requirements. Consequently, the OQE parameter increases with iron content.

The displacement of Fe^{2+} from M2 to M1 caused by heating induces a shortening of the $\langle M2-O \rangle$ bond length following the trend of the natural series.

R^{3+} cation distribution. One of the more interesting questions about the M2 site is: does it host trivalent cations? The answer to this question is very important for its implications in the thermodynamic modelling of the orthopyroxene solution. Ganguly and Ghose (1979) suggested the possibility of a "Opy" component in orthopyroxene with the composition $Mg_3Al_2Si_3O_{12}$ that mixes with $Mg_4Si_4O_{12}$. In such a component during disordering some Al^{VI} is required to occupy the M2 site.

From our plots it appears that in natural orthopyroxenes with some Fe^{2+} in the M2 site, Al^{VI} does not enter that site. This conclusion is based on the following observations:

(1) Unlike M1-O bond distances, the four short M2-O bond lengths do not decrease with increasing R^{3+} content in the unit formula: on the contrary two of them (M2-O1A and M2-O2A) increase as explained above.

(2) Among the longest bond distances, M2-O3A does not vary with R^{3+} content: therefore the shortening of M2-O3B can not be ascribed to the entry of R^{3+} cations into M2 but must be caused by charge balance requirements of O3B, which is linked to two TB sites where some Si/ Al^{IV} substitution takes place.

A general statement regarding the systematic absence of

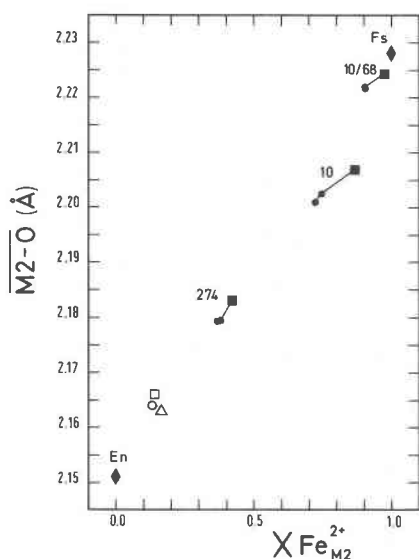


Fig. 8. Variation of mean M2-O bond length with Fe^{2+} content of M2 site. Same symbols as for Fig. 3.

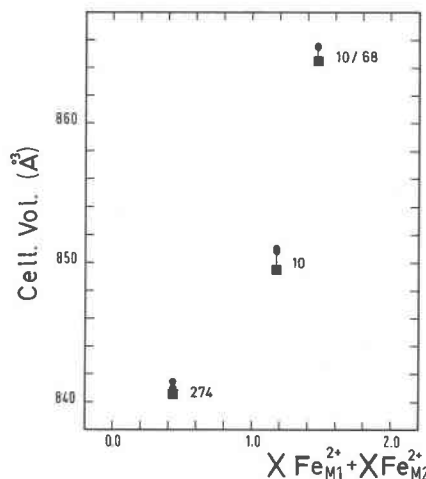


Fig. 9. Variation of unit cell volume with total Fe^{2+} content. Same symbols as for Fig. 3.

R^{3+} in the M2 site of natural orthopyroxenes requires further confirmation of X-ray crystal-chemical study on a series of aluminous samples. Such a study is in progress.

It can be noted that "Opy" may not be a real component according to the present data but its use as a component of orthopyroxene solid solution as proposed by Ganguly and Ghose (1979) is still possible if it is defined as a fictive component (Saxena, 1982).

Unit-cell parameters

The a , b and c unit-cell parameters increase with Fe content according to the data of Brown (1967). The plot of Figure 9 displays the increase of the unit-cell volume with Fe^{2+} -total in the 274, 10 and 10/68 samples, natural and heated. The heating, which displaces the larger Fe^{2+} ions from M2 to M1, induces a small but significant increase in unit-cell volume. This emphasizes the major effect of the polyhedron M1 in determining the dimensions of the entire octahedral layer and allows one to estimate the contribution of disordering to the thermal expansion in orthopyroxenes.

Conclusions

The main original results of this study on the structural changes in *Pbca* orthopyroxenes as a function of chemical composition and Mg^{2+} - Fe^{2+} distribution are the following:

(1) The mean T-O distance in TA and TB tetrahedra are not significantly affected by the chemical composition of the neighboring octahedral sites; therefore any change of $\langle TB-O \rangle$ distance may provide a measure of Si/ Al^{IV} substitution at the TB site.

(2) Our data indicate that R^{3+} cations, entering the structure with the Si/ Al^{IV} substitution, are totally ordered at the M1 site.

(3) The mean bond distance M2-O increases with iron content of the M2 site; this linear relationship is due to a

sum of complementary trends of the individual bond distances. The longest distances, M2-O3, which are controlled in part by M2 and in part by M1 site population, increase with the expansion of the entire octahedral layer. The slight charge deficit at the M2 site due to the large increase of M2-O3A and M2-O3B in the more Fe-rich samples is balanced by a contraction of the other M2-O distances. In this way the M2 site exhibits a 4 + 2 coordination.

(4) The unit-cell volume increases slightly with Mg^{2+} - Fe^{2+} disorder induced by heating.

Acknowledgments

We are grateful to Prof. S. K. Saxena for discussion, helpful suggestions and improvements of the paper. We also wish to thank Prof. S. Ghose for his comments and Dr. A. Cundari for revising the manuscript. Financial support was provided by C.N.R. (Centro di Studio per la Cristallografia Strutturale, Pavia; Centro di Studio sui Problemi dell'Orogeno delle Alpi Orientali, Padova) and by Ministero della Pubblica Istruzione.

References

- Brown, G. M., (1967) Mineralogy of basaltic rocks. In H. H. Hess and A. Poldevaart, Eds., *Mineralogy of Basaltic Rocks. I, Basalt*, p. 103-162. Interscience, New York.
- Busing, W. R., Martin, K. O., and Levy, H. S. (1962) ORFLS, a Fortran crystallographic least-squares program. U.S. National Technical Information Service, ORNL-TM-305.
- Butler, P., Jr. (1969) Mineral compositions and equilibria in the metamorphosed iron formation of the Gagnon region, Quebec, Canada. *Journal of Petrology*, 10, 56-101.
- Cameron, M. and Papike, J. J. (1981) Structural and chemical variations in pyroxenes. *American Mineralogist*, 66, 1-51.
- Cannillo, E., Germani, G., and Mazzi, F. (1983) Nuovo software cristallografico per il diffrattometro a cristallo singolo Philips PW 1100 (New crystallographic software for Philips PW 1100 single crystal diffractometer). C.N.R., Centro di Studio per la Cristallografia Strutturale, Internal Report 2-1983.
- Colby, J. W. (1972) "MAGIC IV, a computer program for quantitative electron microprobe analysis". Bell Telephone Laboratories, Inc. Allentown, Pennsylvania.
- Coppens, P. and Hamilton, W. C. (1970) Anisotropic extinction in the Zachariasen approximation. *Acta Crystallographica*, A26, 71-83.
- Ganguly, J. and Ghose, S. (1979) Aluminous orthopyroxene: order-disorder, thermodynamic properties and petrologic implications. *Contributions to Mineralogy and Petrology*, 69, 375-385.
- International Tables for X-ray Crystallography (1974) Kynoch Press, Birmingham G.B., Vol IV, 99-101.
- Morimoto, H. and Koto, K. (1969) The crystal structure of orthoenstatite. *Zeitschrift für Kristallographie*, 129, 65-83.
- North, A. C. T., Phillips, D. C., and Mathews, F. S. (1968) A semi-empirical method of absorption correction. *Acta Crystallographica*, A24, 351-359.
- Papike, J. J., Cameron, K. L., and Baldwin, K. (1974) Amphiboles and pyroxenes: Characterization of *Other* than quadrilateral components and estimates of ferric iron from microprobe data. *Geological Society of America Abstracts with Programs*, 6, 1053-1054.
- Pauling, L. (1960) *The Nature of the Chemical Bond* (3rd. ed.). Cornell University Press, Ithaca, New York.
- Robinson, K., Gibbs, G. V., and Ribbe, P. H. (1971) Quadratic elongation, a quantitative measure of distortion in coordination polyhedra. *Science*, 172, 567-570.
- Rossi, G., Smith, D. C., Ungaretti, L., and Domeneghetti, M. C. (1983) Crystal-chemistry and cation ordering in the system diopside-jadeite: a detailed study by crystal structure refinement. *Contributions to Mineralogy and Petrology*, 83, 247-258.
- Saxena, S. K. (1968) Chemical study of phase equilibria in charnockites, Varberg, Sweden. *American Mineralogist*, 53, 1674-1695.
- Saxena, S. K. and Ghose, S. (1971) Mg^{2+} - Fe^{2+} order-disorder and the thermodynamics of the orthopyroxene crystalline solution. *American Mineralogist*, 56, 532-559.
- Saxena, S. K. (1982) Computation of multicomponent phase equilibria. *Advances in Physical Geochemistry*, Vol. 2. Springer-Verlag, New York.
- Smyth, J. R. (1973) An orthopyroxene structure up to 850°C. *American Mineralogist*, 58, 636-648.
- Sueno, S., Cameron, M., and Prewitt, C. T. (1976) Orthoferrosilite: high-temperature crystal chemistry. *American Mineralogist*, 61, 38-53.
- Thompson, J. B. (1970) Geometrical possibilities for amphibole structures: model biopyriboles. *American Mineralogist*, 55, 292-293.
- Tokonami, M. (1965) Atomic scattering factor for O^{2-} . *Acta Crystallographica*, 19, 486.

*Manuscript received, August 10, 1984;
accepted for publication, April 21, 1985.*